JPE 18-2-20

https://doi.org/10.6113/JPE.2018.18.2.533
ISSN(Print): 1598-2092 / ISSN(Online): 2093-4718

Constant Output Power Control Methods for Variable-Load Wireless Power Transfer Systems

Xu Liu[*], Lindsay Clare[**], Xibo Yuan[*,**], Jun Wang[**], Chonglin Wang[*], and Jianhua Liu[†]

[†,*]School of Electrical and Power Engineering, China University of Mining and Technology, Xuzhou, China
[**]Electrical Energy Management Research Group, University of Bristol, Bristol, UK

Abstract

This study proposes a comprehensive mathematical model that includes coil-system circuit and loss models for power converters in wireless power transfer (WPT) systems. The proposed model helps in understanding the performance of WPT systems in terms of coil-to-coil efficiency, overall efficiency, and output power capacity and facilitates system performance optimization. Three methods to achieve constant output power for variable-load systems are presented based on system performance analysis. An optimal method can be selected for a specific WPT system by comparing the efficiencies of the three methods calculated with the proposed model. A two-coil 1 kW WPT system is built to verify the proposed mathematical model and constant output power control methods. Experimental results show that when the load resistance varies between 5 and 25 Ω, the system output power can be maintained at 1 kW with a maximum error of 6.75% and an average error of 4%. Coil-to-coil and overall efficiencies can be maintained at above 90% and 85%, respectively, with the selected optimal control method.

Key words: Constant output power, Optimized efficiency, System performance effect factors, Wireless power transfer systems

I. INTRODUCTION

Wireless power transfer (WPT) systems transfer energy from a power source to isolated loads across a large air gap through an alternating magnetic field and have been investigated since the significant contribution of Nikola Tesla in the early 1900s [1]. WPT systems can significantly enhance the flexibility and safety of electrical equipment because of the elimination of physical contact between the source and load. Therefore, this technology has been an active research topic and widely used in implantable devices [2], [3], electric vehicles (EVs) [4]-[7], and portable devices [8], [9] to power up devices or temporarily recharge their batteries. With the rapid development of EVs, high-power WPT systems for charging EV batteries are in urgent demand and need to meet different charging criteria, such as constant voltage charging [10], [11], constant current charging [12], and constant power charging [13]. In WPT systems, powering up different electrical equipment with variable load resistance but at a similar power level is useful for practical purposes.

WPT systems are based on magnetic resonance coupling technology [14]-[18], and their coil systems are composed of at least two coils, namely, transmit and receive coils [19]-[21]. These coils are separated by an air gap, the length of which depends on the requirements of electrical equipment (e.g., 100 mm to 300 mm for charging EVs). The coupling coefficient between transmit and receive coils is small and typically ranges from 5% to 30% because of the large air gap between the two coils and the alignment and structure of the coils [22]. This small coupling coefficient leads to low mutual inductance and high leakage inductance between the two coils. A compensation circuit is usually applied to cancel leakage inductance because energy is transferred through mutual inductance, and leakage inductance provides no direct contribution to active power transfer [23]. Compensation capacitors, which can be lumped or parasitic, are usually added to form a compensation circuit to resonate with the coils [24]. This approach is called the magnetic resonance method. The four basic compensation topologies, namely, series–series (SS), series–parallel, parallel–series, and parallel–parallel, dep end on how the coils are compensated for by the capacitors [24], [25]. In this study, the basic SS compensation

Manuscript received Jun. 16, 2017; accepted Dec. 12, 2017
Recommended for publication by Associate Editor Yijie Wang.
[†]Corresponding Author: liujianhua@cumt.edu.cn
Tel: +86-0516-83885605, China University of Mining and Technology
[*]Sch. Electrical Power Eng., China Univ. Mining Tech., China
[**]Electrical Energy Management Research Group, Univ. of Bristol, UK

topology is selected because of its simple structure, but the analysis is also applicable to other compensation topologies.

The primary design objectives of WPT systems are to increase power transfer capacity and improve power transfer efficiency [26]. Fig. 1 shows the functional blocks of a typical experimental WPT system. Overall efficiency is the power efficiency from the load to the power source, and coil-to-coil efficiency is the power efficiency from the secondary-side coil system (input power to the rectifier) to the primary-side coil system (output power from the inverter). The power transfer capacity and efficiency of transmit and receive coils are affected by the resonant frequency, coupling coefficient, and load impedance of the system. The overall efficiency of the system is also affected by losses from power converters, the iron core, and equivalent series resistances (ESRs) of resonators. Impedance matching is commonly used to maximize the power transferred in many radio frequency circuit designs, and it is implemented when the input resistance of the inverter is equal to the internal resistance of the power source. However, the overall efficiency of an impedance-matched WPT system is limited to 50% [26], [27]. Soft-switching, wide-bandgap semiconductor power devices, such as GaN or SiC metal–oxide–semiconductor field-effect transistors (MOSFETs), are adopted to reduce the losses in power converters and improve the overall system efficiency. Using a low resonant frequency is another approach to reduce the losses in power converters and the iron core, but in several electrical equipment, resonance frequency is limited to a certain value, such as 85 kHz for charging EVs [28]. Litz wires are commonly used to reduce the AC resistance of coils, and film capacitors are utilized for their low ESR properties. The coil-to-coil efficiency of WPT systems has been analyzed in detail, but the overall efficiency of WPT systems, including that of the inverter and load rectifier, has received minimal attention; only several studies can be found in existing literature (e.g., [29]-[31]). The current study is different from [29]-[31]. The equivalent resistances of the rectifier, filter, and resistor circuit are analyzed to simplify the circuit analyses in our work and in [29]-[31]. However, in our work, detailed calculations of switching device losses in the inverter and rectifier are presented to derive a full and precise mathematical model of an entire WPT system. Moreover, when system efficiency is improved by applying several methods [2], the changes in output power are sometimes given minimal attention. An inherent characteristic of WPT systems is that they produce constant current or voltage with careful design of the value of the compensation capacitors. For example, the SS compensation topology can provide a constant voltage output if the capacitor is designed to resonate with the coil leakage inductance, but it produces a constant current output when the capacitors are designed to resonate with the coil self-inductance [32]. However, research on constant output power systems, which are required in many general applications and several battery-charging ones, remains lacking [13], [33], [34]. Research on constant power control methods helps in achieving constant power charging for variable-load systems and understanding the basic characteristics of WPT systems to improve WPT efficiency.

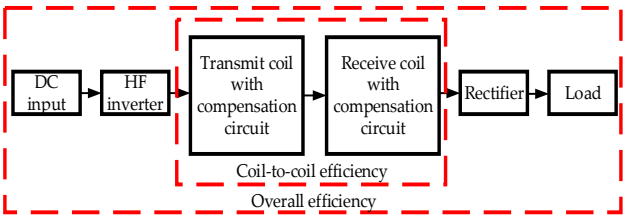

Fig. 1. Function blocks of the WPT systems in this work.

A comprehensive mathematical model of the entire system that includes coil system circuit and loss models of the power converters is derived in this study. The factors that affect WPT system performance in terms of coil-to-coil efficiency (η_{cc}), overall efficiency (η_{dd}), and output power (P_L) are analyzed with the proposed comprehensive mathematical model. A control strategy that includes three constant output power control methods for variable load resistance WPT (VLWPT) systems is presented based on the analysis of WPT performance. The results show that with the proposed mathematical model, the output power of the WPT system can be maintained with high efficiency.

II. Theoretical Analysis

The objective of this section is to construct a precise and comprehensive mathematical WPT system model that can help designers establish new WPT systems with specific requirements and predict the performance of these systems. This section deals first with modelling of the transmit and receive circuits, and then with the loss model of the power converters in the WPT system.

A. Coil System Circuit Model

A circuit diagram of the WPT system is shown in Fig. 2(a). The primary coil system consists of transmit coil L_1 and its series-connected compensation capacitor C_1. The primary coil system is driven by a high-frequency voltage source inverter that applies a square-wave voltage to the L_1–C_1 resonant circuit. The primary side is made resonant to reduce the *V*/*A* required to set up the required primary current. The circuit is purely resistive at the fundamental frequency but has high inductive reactance to harmonics; as a result, the current flowing through the L_1–C_1 resonant circuit is sinusoidal at the fundamental frequency. This current generates a magnetic field around the transmit coil, which induces a voltage in the receive coil by mutual inductance. The induced voltage can be rectified to provide DC power to a load. The compensation capacitor on the secondary side, C_2, cancels out the inductive reactance of the secondary coil, which would otherwise

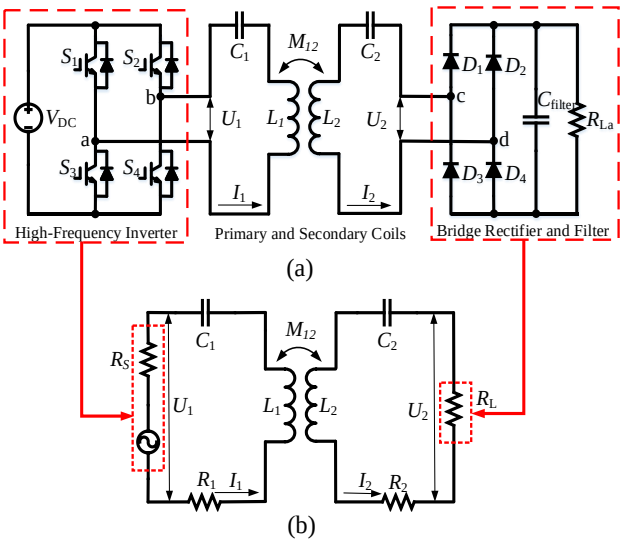

Fig. 2. WPT system. (a) Entire system. (b) Simplified model.

seriously limit the load current. Capacitor C_f at the rectifier output bypasses ripple current at switching and harmonic frequencies from the load. When the system is used to charge EVs, the load is the EV batteries. In this manner, transfer of electrical energy through the air from the transmit coil to the receive coil is achieved [29], [35].

The circuit in Fig. 2(a) can be simplified to the equivalent model in Fig. 2(b), where $\boldsymbol{U_1}$ is the output voltage phasor of the high-frequency inverter applied to the primary coil system and $\boldsymbol{U_2}$ is the output voltage phasor of the secondary coil system and the input voltage to the H-bridge rectifier. The H-bridge rectifier, filter capacitor, and actual load R_{L_a} are regarded as equivalent resistance R_L. In this simplified model, R_1 and R_2 are the parasitic resistances in the primary and secondary sides, respectively, and they consist of the resistances of the coils and compensation capacitors. The equivalent resistance of a capacitor can be derived from its dissipation factor $\tan\delta$, which is obtained from the datasheet for the capacitor using $\mathrm{ESR} = \tan\delta/2\pi fC$. For example, for a 33 nF capacitor with $\tan\delta$ = 3*e*-3 at 85 kHz, ESR = 170 mΩ. When capacitors are assembled in series – parallel units, the resultant ESR of the unit is approximately obtained from the calculation of the ESRs in series and parallel. However, to ensure accuracy, a Wayne Kerr 6500B analyzer is used in the experiments to measure the total parasitic resistance of the connected coil and its corresponding compensation capacitor. $\boldsymbol{I_1}$ and $\boldsymbol{I_2}$ are the current phasors for the primary and secondary sides, respectively. The secondary-side series resonant circuit forces a sinusoidal current through the rectifier, which results in square-wave voltage $\boldsymbol{U_2}$ at the rectifier input. The RMS value of the fundamental component of the square voltage waveform is $2\sqrt{2}/\pi$ of its peak value. At the rectifier output, the voltage across output capacitance C_f and load R_{L_a} is nearly constant with a small ripple component, and it is approximately equal to the input square-wave voltage minus the rectifier drop. When the WPT system operates at resonance, the input voltage and current at the rectifier on the secondary side are in phase. Under this condition, power transfer is the product of the RMS value of the sinusoidal current and the RMS value of the fundamental component of the square voltage waveform while assuming 100% power efficiency. According to the law of energy conservation, Eqs. (1) to (5) can be easily derived, thus allowing the relationship between actual and equivalent loads to be expressed as Eq. (6).

$$P_{rectifier\ input} = P_{rectifier\ output} \tag{1}$$

$$R_{La} = \frac{V_L^2}{P_{rectifier\ output}} \tag{2}$$

$$R_L = \frac{U_{2\_RMS}^2}{P_{rectifier\ input}} \tag{3}$$

$$V_L = U_{2\_AMP} \tag{4}$$

$$U_{2\_RMS} = (2\sqrt{2}/\pi)U_{2\_AMP} \tag{5}$$

$$R_L \cong 0.81R_{L_a} \tag{6}$$

For a resonant WPT system, the compensation capacitance is selected to resonate with the self-inductance of the coil at a specific resonant frequency, as expressed in Eqs. (7) and (8).

$$C_1 = 1/(\omega_r^2 L_1), \tag{7}$$

$$C_2 = 1/(\omega_r^2 L_2), \tag{8}$$

where ω_r is the resonant angular frequency.

With the lumped-element circuit shown in Fig. 2(b), the WPT system can be expressed in a matrix form according to KVL as follows [24]:

$$\begin{bmatrix} \overrightarrow{U_1} \\ 0 \end{bmatrix} = \begin{bmatrix} Z_1 & j\omega_d M_{12} \\ j\omega_d M_{12} & Z_2 \end{bmatrix} \begin{bmatrix} \overrightarrow{I_1} \\ \overrightarrow{I_2} \end{bmatrix}, \tag{9}$$

where $Z_1 = R_S + R_1 + j\omega_d L_1 - j/(\omega_d C_1)$ is the impedance of the primary side, $Z_2 = R_L + R_2 + j\omega_d L_2 - j/(\omega_d C_2)$ is the impedance of the secondary side, R_S is the equivalent resistance of the inverter, and ω_d is the driving angular frequency.

Therefore, the current vector in the primary and secondary sides can be derived from Eq. (9).

$$\overrightarrow{I_1} = \frac{Z_2 \overrightarrow{U_1}}{\omega_d^2 M_{12}^2 + Z_1 Z_2} \tag{10}$$

$$\overrightarrow{I_2} = \frac{-j\omega_d M_{12} \overrightarrow{U_1}}{\omega_d^2 M_{12}^2 + Z_1 Z_2} \tag{11}$$

The power injected into the primary side (P_{pri}), the power delivered to the load (P_{sec}), and the coil-to-coil efficiency (η_{cc}) can be expressed as follows:

$$P_{pri} = \overrightarrow{U_1}\overrightarrow{I_1} = \frac{Z_2 \overrightarrow{U_1}^2}{\omega_d^2 M_{12}^2 + Z_1 Z_2}, \tag{12}$$

$$P_{sec} = \overrightarrow{I_2}^2 R_L = \left(\frac{-j\omega_d M_{12} \overrightarrow{U_1}}{\omega_d^2 M_{12}^2 + Z_1 Z_2}\right)^2 R_L, \tag{13}$$

$$\eta_{coil-coil} = \frac{P_{sec}}{P_{pri}} = \frac{\omega_d{}^2 M_{12}{}^2 R_L}{(\omega_d{}^2 M_{12}{}^2 + Z_1 Z_2) Z_2}. \tag{14}$$

Losses due to the inverter and rectifier need to be calculated to determine the overall efficiency. Detailed analyses are presented in the subsequent subsection.

When the WPT system operates under resonant conditions, that is, when the driving frequency equals the resonant frequency as expressed in Eqs. (15) and (16), the primary- and secondary-side impedances can be calculated using Eqs. (17) and (18).

$$f_d = f_r \tag{15}$$

$$\omega_d = \omega_r = 2\pi f_r \tag{16}$$

$$Z_1 = R_S + R_1 \tag{17}$$

$$Z_2 = R_L + R_2 \tag{18}$$

Although square-wave voltage excitation is applied to the circuit on the primary side, the coil current is sinusoidal because the circuit has high impedance at harmonic frequencies but is purely resistive at the fundamental frequency. On the secondary side, the rectifier and load are part of a series resonant circuit, which forces the rectifier input current to be sinusoidal. Therefore, fundamental harmonic approximation can be used to analyze the working principle. The power transferred to the primary side and the power received by the secondary side can be expressed as follows:

$$P_{pri_{\omega=\omega_r}} = \overrightarrow{U_1}\overrightarrow{I_1} = U_1 I_1, \tag{19}$$

$$P_{sec_{\omega=\omega_r}} = \overrightarrow{I_2}^2 R_L = {I_2}^2 R_L. \tag{20}$$

By substituting Eqs. (10) and (11) into Eqs. (14), (19), and (20), P_{pri}, P_{sec}, and η_{cc} can be expressed as Eqs. (21) to (23), respectively, under resonant conditions. Eq. (23) shows that the coil-to-coil efficiency is related to the resonance/driving frequency, load resistance, mutual inductance, and parasitic resistance of the coil system.

$$P_{pri_{\omega=\omega_r}} = \frac{{U_1}^2(R_L + R_2)}{{\omega_d}^2{M_{12}}^2 + (R_S + R_1)(R_L + R_2)} \tag{21}$$

$$P_{sec_{\omega=\omega_r}} = \frac{{\omega_d}^2{M_{12}}^2{U_1}^2 R_L}{({\omega_d}^2{M_{12}}^2 + (R_S + R_1)(R_L + R_2))^2} \tag{22}$$

$$\eta_{cc} = \frac{{\omega_d}^2{M_{12}}^2 R_L}{({\omega_d}^2{M_{12}}^2 + (R_S + R_1)(R_L + R_2))(R_L + R_2)} \tag{23}$$

B. Loss Model of the Power Converters

Losses due to the primary-side inverter and secondary-side rectifier need to be calculated to determine the overall efficiency of the WPT system. The power devices in the primary-side, single-phase, two-level DC–AC inverter incur conduction and switching losses. The optimization conducted in this work is based on SiC MOSFETs (Cree C2M00 40120D), and conduction losses only exist in the MOSFET channel and body diode when the switching dead-time periods are ignored. For MOSFETs, synchronous conduction is normally used to reduce the conduction loss, which means the MOSFET channel instead of the body diode conducts the current when reverse current flows. Therefore, the conduction loss is expressed in Eq. (24).

$$P_{con} = \frac{1}{T}\int_0^{T/2} (\widehat{I_1}\sin(\omega t))^2 R_{ds} dt, \tag{24}$$

where T is the switching period of the MOSFETs, $\widehat{I_1}$ is the drain current of the MOSFETs, and R_{ds} is the on-state resistance of the MOSFETs.

The turn-on and turn-off losses can be derived from the relationship between switching energy and drain current from the datasheet and can be expressed as Eq. (25). The reverse recovery loss can also be calculated using the reverse recovery charge from the datasheet, as expressed in Eq. (26) [36], [37].

$$\begin{aligned} P_{switching} &= \frac{V_{DC}}{V_{CC}} f_d \int_0^T \left(P_{on} + P_{off}\right) dt \\ &= \frac{V_{DC}}{V_{CC}} f_d (E_{on} + E_{off}), \end{aligned} \tag{25}$$

$$P_{rr} = \frac{f_d V_{dc} Q_{rr}}{\pi} \frac{\widehat{I_1}}{I_{CC}}, \tag{26}$$

where Q_{rr} is the reverse recovery charge, I_{CC} is the test current of the device, E_{on} is the turn-on energy loss given in the datasheet, and E_{off} is the turn-off energy loss given in the datasheet.

A pair of MOSFETs conduct simultaneously in one switching cycle. Therefore, the total loss in the inverter is

$$P_{inverter} = 2\left(P_{con} + P_{switching} + P_{rr}\right). \tag{27}$$

Power loss is mainly composed of the conduction losses and the reverse recovery loss in the rectifier Schottky diode, as expressed in Eqs. (28) and (29), respectively, where V_F is the diode forward voltage drop, I_2 is conduction current, and V_0 is the diode reverse voltage, which is equal to the amplitude of $\boldsymbol{U_2}$ minus the diode forward voltage drop, and is therefore approximately equal to the amplitude of $\boldsymbol{U_2}$. R_{on} is the on-state resistance of the diode.

$$\begin{aligned} P_{d\_cond} &= \frac{1}{T}\int_0^T V_F \cdot I_2(t) dt \\ &= \frac{1}{T}\int_0^T (V_0 \cdot I_2(t) + R_{on} I_2^2(t)) dt \end{aligned} \tag{28}$$

$$P_{d\_rr} = \frac{f_d V_{dc} Q_{rr}}{\pi} \frac{\widehat{I_2}}{I_{CC}} \tag{29}$$

A pair of rectifier diodes conduct in one switching cycle, such that the power loss for the rectifier can be expressed in Eq. (30).

$$P_{rectifier} = 2\left(P_{d\_cond} + P_{d\_rr}\right) \tag{30}$$

With the calculated losses of the inverter and rectifier, the DC input power, DC load power, and overall efficiency can be approximately expressed as Eqs. (31) to (33), respectively.

$$P_{DC} = P_{pri} + P_{inverter} \tag{31}$$

$$P_L = P_{sec} - P_{rectifier} \tag{32}$$

$$\eta_{dd} = P_L / P_{DC} \tag{33}$$

III. Effects of System Parameters on WPT System Performance

To design a WPT system with specific requirements (e.g., constant output power in this work), WPT system performance should be studied to determine the factors that affect the coil-to-coil efficiency, overall efficiency, and output power of a two-coil resonant WPT system. According to their respective equations derived in Section II, load power, coil-to-coil efficiency, and overall efficiency are affected by input DC voltage, resonant frequency, driving frequency, load resistance, coil parameters, and coupling coefficient between the two coils.

A two-coil WPT system capable of 3.5 kW operation is built, as shown in Fig. 3, to validate the mathematical model of WPT systems and the subsequent analysis. An EA-PS 81000-30 DC power supply is used to power the system. An H-bridge inverter is employed to excite the transmit coil, with SiC MOSFETs (Cree C2M0040120D) as the switching devices. An H-bridge rectifier formed by SiC fast-recovery diodes (Cree C4D20120) with a parallel-connected filter capacitor (EPCOS (TDK), B32778G8606J000) is utilized to rectify the received AC power to provide DC power to the load resistors. Two NORMA 4000 power analyzers are used to measure the DC input power, inverter output power, rectifier input power, and load power. The range of load resistance (TE connectivity of 1 kΩ, 1 kW each resistor) used in this work is between 5 and 25 Ω and is of a similar order to that used in various other work dealing with IPT systems for battery charging [38]-[42]. SP-connected film capacitors with various values (EPCOS (TDK)) are adopted as compensation capacitors and arranged to provide the required capacitance value without exceeding the AC voltage rating of individual capacitors at the operating frequency.

Fig. 4 shows the plan view of the coil used in this work. The design parameters of the coils used in this study are shown in Tables I and II. The Litz wire is manufactured in-house and composed of 60 × 0.53 mm-diameter enameled copper wire conductors to provide an external diameter of 5 mm. With the aid of finite element analysis (FEA) software (e.g., ANSOFT Maxwell), the simulated and measured self-inductances and AC resistances at 85 kHz are shown in Table III. From the matrix shown in Eq. (9), mutual inductance can be calculated using Eq. (34) when the load resistance, stray resistance, driving frequency, primary voltage, and current are known. When measuring the mutual inductance in the experiments, current sense resistors (MP9100-10.0-1%) replace the rectifier and power resistors to provide an accurate secondary-side impedance. Different DC input voltages and load resistances are adopted in the experiments to derive an average coupling coefficient, which can be considered the final measured coupling coefficient. An alternative method, that presented in [43], may be suitable for a practical WPT system because it measures mutual inductance from measurements on the transmit side only without making any changes to the secondary-side circuit. However, the first method is adopted in this work in a laboratory environment because it is precise and convenient. Fig. 5 shows a comparison of simulated and measured coupling coefficients with a variation in coil-to-coil spacing. The simulation results are in good accordance with the measured results. Therefore, thisFEA analysis allows a designer to obtain an accurate prediction of coil system parameters.

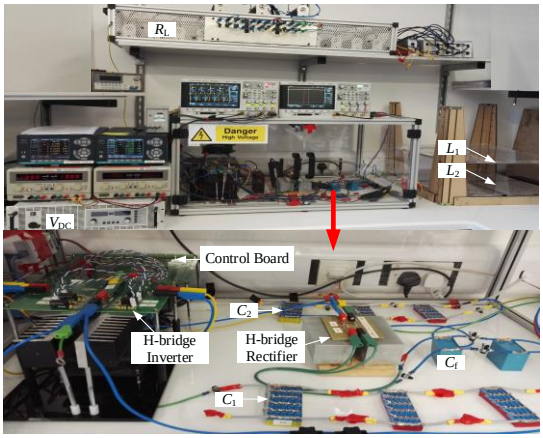

Fig. 3. Experimental platform of the WPT system.

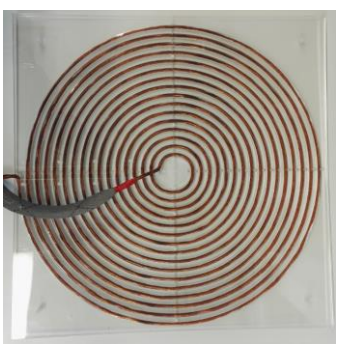

Fig. 4. 16-turn flat spiral coil.

TABLE I
Litz Wire Parameters

Single conductor diameter	Number of conductors	Overall Litz wire diameter
0.53 mm	60	5 mm

TABLE II
Coil Design Parameters

Inner radius	Outer radius	Channel width	Coils turns
30 mm	286 mm	10 mm	16

TABLE III
Coil System Parameters

	Measurement	Simulation
L_1 (μH)	66.575	65.43
R_{L1} (mΩ)	122	107

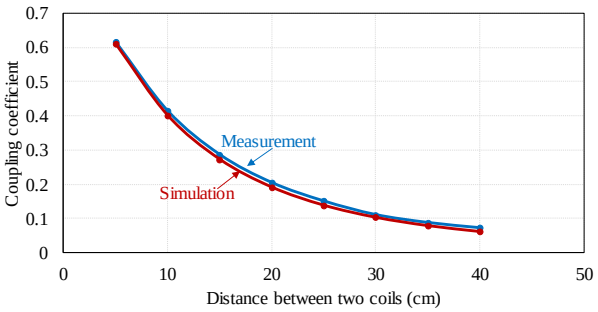

Fig. 5. Coupling coefficient with different coil-to-coil distances.

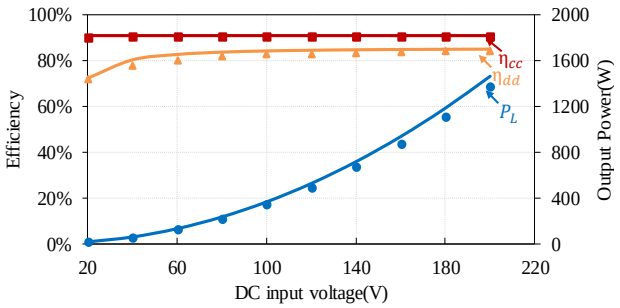

Fig. 6. Effect of DC input voltage on system performance.

TABLE IV
WPT SYSTEM PARAMETERS

Parameter	Value	Unit
V_{DC}	0–200	V
fd	85	kHz
fr	85	kHz
L_1	65.96	μH
C_1	53.2	nF
R_1	138	mΩ
L_2	66.58	μH
C_2	52.5	nF
R_2	142	mΩ
d	50–400	mm
R_{La}	5–25	Ω
P_L	1	kW

$$M_{12} = \sqrt{\frac{\left(\frac{U_1}{I_1} - Z_1\right) Z_2}{{\omega_d}^2}} \tag{34}$$

Usually, the size of the receive coil is limited by the space available in the equipment being supplied. By contrast, the area of the transmit coil may be less constrained, allowing it to be increased to improve coupling and reduce sensitivity to misalignment. However, this work focuses on the effect of system parameters, that is, load resistance, resonant frequency, driving frequency, and coil-to-coil distance. Therefore, identical coils for transmit and receive are used to simplify the calculations and facilitate bidirectional WPT when a controllable inverter instead of a passive rectifier is adopted in the secondary side. In literatures, identical coils are widely adopted in studies on WPT systems to simplify the analysis [44]-[46]. The main parameters used in this work are shown in Table IV.

A. *Effect of DC Input Voltage*

For a WPT system with a given DC input voltage, coil-to-coil distance, and driving frequency, the current in the primary and secondary sides and the voltage in the secondary side vary with different load resistances. Moreover, the losses caused in the power converters are relevant to the voltage and current in the primary and secondary sides. By referring to the mathematical WPT model presented in Section II, it can be found that the losses in the rectifier and inverter influence the overall efficiency. Therefore, the effect of the DC input voltage needs to be considered to determine the required voltage level.

The coil-to-coil vertical distance is set to 150 mm, which is a typical vehicle chassis height, and load resistance is set to 5 Ω. The system operates at a resonance frequency of 85 kHz, which is the operating frequency recommended by SAE J2954 [28] for wireless charging of EV batteries. The DC input voltage is increased from 20 V to 200 V in steps of 20 V to show the effect of DC input voltage on WPT system performance.

Fig. 6 shows the system performance with different DC input voltages. The solid lines denote the results calculated from the mathematical model, and the markers denote the measured results. The two results are in close agreement. Fig. 6 also shows that output power P_L (blue line and markers) increases with the increase in the DC input voltage. The coil-to-coil efficiency (red line and markers) remains constant because coil-to-coil efficiency is unrelated to the DC input voltage, as shown in Eq. (23). The overall efficiency (orange line and markers) initially increases when the DC voltage is low and subsequently flattens out after the DC input voltage increases to 100 V. This result can be attributed to the losses in the inverter and rectifier that dominate the overall losses when the input and output power are low. However, with the increase in power, the inverter and rectifier losses increase at a slow rate, and the dominant factor in the overall efficiency becomes coil-to-coil efficiency. Therefore, in subsequent work, the nominal DC input voltage is set to 100 V, but this value can be slightly adjusted to vary the output power without influencing the coil-to-coil efficiency and only slightly affecting the overall efficiency.

B. *Effect of Coupling Coefficient*

Coupling coefficient *k* represents the degree of electromagnetic coupling between the transmit and receive coils. It depends on the structure of the transmit and receive coils and their relative positions. The structure of the coils is normally fixed, but the relative position may vary in practice to allow the load to be placed at any position above the

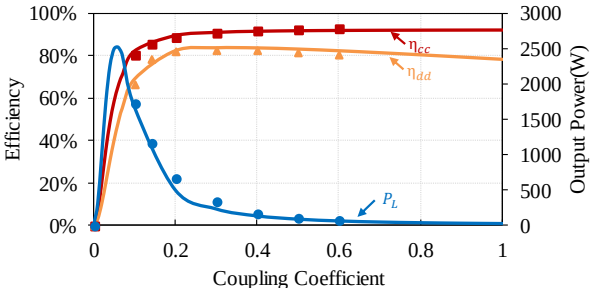

Fig. 7. Effect of coupling coefficient on system performance.

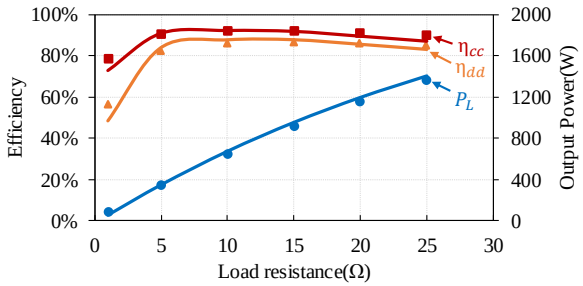

Fig. 8. Effect of load resistance on system performance.

charging surface in a wireless battery-charging platform. In this study, we assume that the two coils are not misaligned, and only the coil-to-coil vertical distance is varied between 50 and 400 mm to simulate various coupling conditions. Coupling can be altered by varying the vertical distance between the two coils, by lateral misalignment, or by angular misalignment. However, the present experimental arrangements allow only the adjustment of the distance between the two coils when they are coaxially aligned. The coupling coefficient with different vertical distance d can be simulated with the FEA software. The load resistance is fixed at 5 Ω in this subsection, and the DC input voltage is held constant at 100 V.

Fig. 7 illustrates that high system efficiency generally corresponds to a high coupling coefficient (small coil-to-coil distance). With regard to the output power, with the increase in coil-to-coil distance, P_L initially increases, reaches a peak, and subsequently decreases. Thus, the maximum value corresponds to one coupling coefficient when the entire system reaches the impedance matching point. The coil-to-coil distance can be optimized in terms of power transfer capacity. However, as can be observed from the curves, the two efficiencies do not reach the maximum at this point. Therefore, high system efficiency can be achieved with a small coil-to-coil distance, but the power transfer capacity is seriously limited. The output power can be varied by adjusting the coil-to-coil distance. In conclusion, when the aim is to achieve the highest system efficiency, the coil-to-coil distance should be as small as possible. By contrast, when the goal is maximum power transfer, the coils should be positioned near the critical coupling point to achieve a system efficiency of approximately 50%. However, for a practical system, the design is likely to be a compromise between efficiency and power transfer capacity.

C. Effect of Load Resistance

In this subsection, the load resistance is changed from 5 Ω to 25 Ω in steps of 5 Ω to analyze the effect of the load on system efficiency. An additional measurement is performed at 1 Ω to obtain a complete plot between 0 and 25 Ω. The coil-to-coil vertical distance is fixed at 150 mm. The results shown in Fig. 8 indicate that although the calculated values have errors, the test trends (as shown by the markers) illustrate good consistency with that predicted by the mathematical model (as shown by the solid lines). The output power approximately increases in a linear manner as the load resistance is increased from 5 Ω to 25 Ω with a constant DC input voltage of 100 V. η_{cc} and η_{dd} increase rapidly, reach a peak, almost flatten out, and continue to decrease slowly.

Notably, if the range of the load resistance is expanded, then the output power does not increase continuously but reaches a peak at a certain R_L and decreases according to the maximum power transfer theorem. This load condition is beyond the scope of this study and is therefore not examined further.

D. Effect of Driving Frequency

Tuning the two coils to exactly the same operating frequency is nearly impossible because of tolerances in the coils and tuning capacitors. In several cases, slightly offsetting the driving frequency to match that of the receive circuit to allow maximum load power may be advantageous. For coil-to-coil distances smaller than the critical coupling distance, twin resonant peaks occur on either side of the resonant frequency even when the primary and secondary circuits are perfectly tuned to the same frequency. This phenomenon is called frequency splitting and has been fully explained in various studies, such as [45], [47], and [48]. Studying the frequency splitting phenomenon is important to achieve highly efficient power transfer and fully utilize the power transfer capacity. In this subsection, the coil-to-coil vertical distance is set to 150, 250, and 350 mm, which are typical vehicle chassis heights. The load resistance is set to 5, 15, and 25 Ω to provide different load conditions. The DC input voltage is kept constant at 100 V.

Figs. 9 and 10 show that the frequency splitting phenomenon occurs when the coil-to-coil distance is sufficiently low (coupling coefficient greater than the critical value) or the load resistance is low. Increasing the coil-to-coil distance or increasing the load resistance eliminates the frequency splitting phenomenon.

When the frequency splitting phenomenon occurs, system efficiency still reaches the maximum at the resonant frequency, whereas the output power decreases to the bottom of the curve at the resonant frequency. The maximum output power is observed at two other driving frequencies, which are

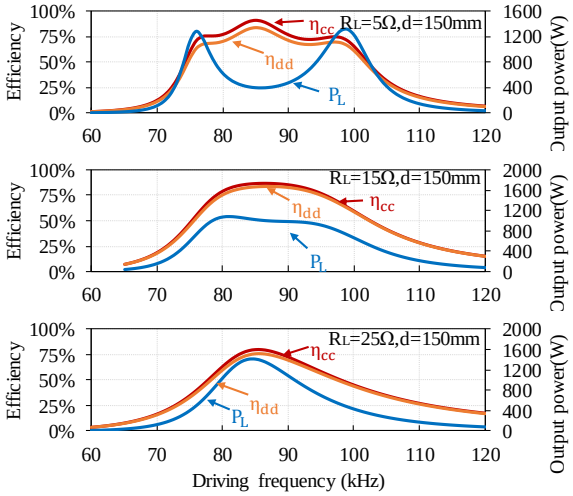

Fig. 9. Effect of driving frequency on system performance with a fixed coil-to-coil distance and various load resistances.

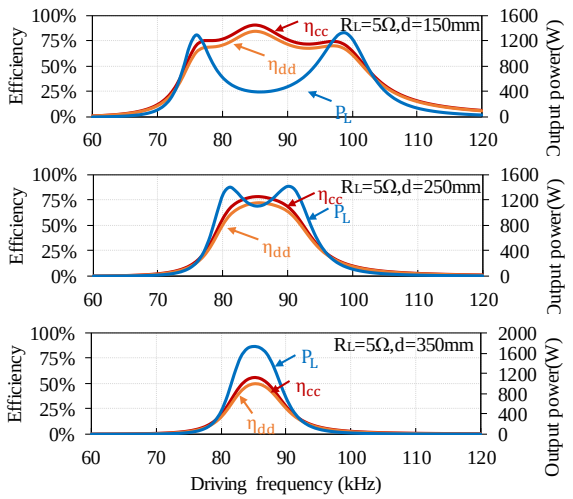

Fig. 10. Effect of driving frequency on system performance with a fixed load resistance and various coil-to-coil distances.

on each side of the resonant frequency (e.g., 76 and 100 kHz in Fig. 9 [R_L = 5 Ω, d = 150 mm], where the resonant frequency is 85 kHz) with slightly reduced system efficiency. In conclusion, when the DC input voltage, load resistance, and coil-to-coil distance are fixed, tuning the driving frequency can adjust the system output power and system efficiency. The power transfer capacity can be significantly increased by utilizing the frequency splitting phenomenon but with a slight reduction in system efficiency. In a practical system, system efficiency and output power are normally considered together, rather than focusing on one to the exclusion of the other.

IV. Study of Constant Output Power Control Methods

The previously presented analysis of SS compensation topology WPT system performance indicates that the output power is dependent on the load resistance. Therefore, for a VLWPT system, if the other parameters of the WPT system are kept constant when the load resistance is varied, then the output power will change. Thus, the front end of the system needs to be tuned to adapt to this requirement to achieve a constant output power. The output power is closely related to the input DC voltage, driving frequency, and coupling coefficient in a two-coil system according to Eq. (13).

The output rectifier uses SiC diodes in a conventional bridge circuit. Rectification efficiency is measured at approximately 95% and observed to vary only slightly between experiments. Therefore, to simplify calculations, the efficiency of the rectifier is regarded as 95% for all calculations. The rectifier input power is derived using Eq. (35).

$$P_{sec} = P_L/0.95 \tag{35}$$

In this work, constant output power is set to 1 kW with variable load resistance from 5 Ω to 25 Ω. All of the required parameters are calculated using the mathematical WPT system model presented in Section II. Based on the system parameter adjustment method to achieve constant output power, a comprehensive method is presented in this work to achieve optimal system efficiency for the VLWPT system.

A. Method A: Adjusting the DC Input Voltage

An approach to achieve constant output power is to control the DC input voltage, as observed from the analysis presented in the previous section. A variable regulated DC power supply is used to allow the input voltage to be set at the desired experimental value. For a practical system, the DC power supply can be replaced with an AC–DC converter and a DC–DC boost/buck converter to provide a stable variable DC input voltage but with a slight loss in efficiency. The output power is proportional to the load resistance and DC input voltage according to the secondary-side power expression shown in Eq. (13). Assuming zero dead time, the root mean square (RMS) value of the fundamental component of a square wave is $2\sqrt{2}/\pi$ of the amplitude of the square wave, as expressed in Eq. (36), and the relationship among input DC voltage, output power, and load resistance can be derived as Eq. (37).

$$2\sqrt{2}/\pi U_{DC} = U_{1_{RMS}} \tag{36}$$

$$\overrightarrow{U_1} = \frac{\sqrt{\frac{P_{sec}}{R_L}}(\omega_d{}^2 M_{12}{}^2 + Z_1 Z_2)}{j\omega_d M_{12}} \tag{37}$$

The coil-to-coil vertical distance is fixed to 150 mm, and the resonant and driving frequencies are fixed to 85 kHz. Based on the calculated DC input voltage using Eqs. (36) and (37), 1 kW constant output power can be effectively maintained with a maximum error of 6.7% (i.e., Error = (measured load power−desired load power)/desired load power). The average error of this method is 4.61% within the

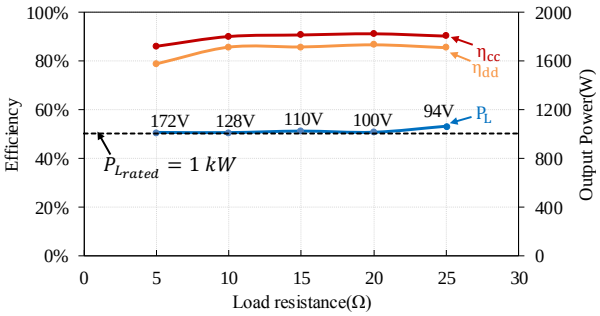

Fig. 11. Experimental results for constant output power by adjusting the DC input voltage.

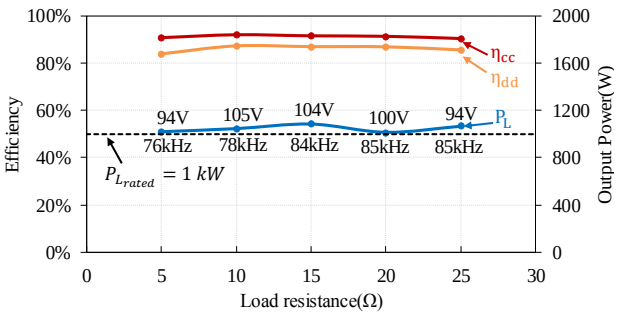

Fig. 12. Experimental results for constant output power by adjusting the DC voltage and driving frequency.

entire range of the load resistance. The error is caused by the assumptions in this work and the non-negligible stray resistance in the leads and connection nodes in the WPT system, particularly for the parasitic resistance in the screws used to connect the components in the WPT system. However, the error does not affect the analysis of the constant output control methods. When the stray resistance existing in the leads and connection nodes can be significantly reduced, precision can be further improved. When the load resistance is increased, the DC link voltage must be reduced, as marked on the curves shown in Fig. 11. In these experiments, the DC input voltage decreases from 172 V to 94 V with the increase in load resistance from 5 Ω to 25 Ω. η_{cc} and η_{dd} initially increase from 86.19% to 90.27% and from 78.86% to 85.81%, respectively, with the increase in load resistance from 5 Ω to 10 Ω; subsequently, they remain nearly constant. However, with the increase in load resistance, the two efficiencies are dominated by the load resistance and present an increase. As analyzed in Section III-A, the DC input voltage does not affect the coil-to-coil efficiency, and when the power level is sufficiently high, the effect on the overall efficiency of the system is only slight. Therefore, with variable load resistance, the change in η_{cc} and η_{dd} can be attributed to the load resistance. When this method is used, these two efficiencies are dominated by the load resistance. The most significant advantage of this method is that η_{cc} and η_{dd} do not change significantly when the load resistance is sufficiently high. However, when the DC voltage is adjusted, the voltage stress on the power devices and compensation capacitors also changes. This finding needs to be carefully considered at high power.

B. Method B: Adjusting the DC Input Voltage and Driving Frequency

When the coupling increases to above the critical coupling, the load power curve changes from a single-peak curve to a double-peak curve and presents a double-peak characteristic. The peak load power given in Eq. (13) is closely related to its partial derivative with respect to system operating frequency. The partial derivative with respect to the system operating frequency of the output power in the secondary side can be derived using Eq. (38) and is called the splitting equation.

$$f_{(fd)} = \frac{\partial P_{sec}}{\partial f_d} = 0 \tag{38}$$

Therefore, if the frequency splitting phenomenon occurs, Eq. (38) will have three solutions, that is, $f_{Ridege+}$, $f_{Ridege-}$, and f_{Trough} [45]. The first two values are the two peak values on either side of the resonance frequency point. f_{Trough} corresponds to the trough value of the output power wave and equals the system resonant frequency. The driving frequency can be converted to $f_{Ridege+}$ or $f_{Ridege-}$ to achieve the maximum power transfer capacity. A low driving frequency can reduce the losses in the inverter and rectifier. Therefore, in this case, $f_{Ridege-}$ is selected to be the tuning objective of the driving frequency, with the input DC voltage being adjusted to achieve the desired output power. When Eq. (38) has only one solution, the frequency splitting phenomenon disappears, and the output power attains its peak at the resonant frequency.

Method B is also validated by experiments, and the results are shown in Fig. 12. The coil-to-coil vertical distance is still set to 150 mm, the resonant frequency is 85 kHz, the DC input voltage is held constant at 100 V, and the load resistance is increased from 5 Ω to 25 Ω in 5 Ω steps. The maximum and constant output power can be achieved in the system, as shown in Fig. 12, with a maximum error of 6.73% and an average error of 2.46%. The adjusted DC input voltages and driving frequencies corresponding to each load resistance are marked on the lines. With the increase in load resistance from 5 Ω to 25 Ω, η_{cc} and η_{dd} initially increase and subsequently keep nearly constant at 90% and 85%, respectively. The analysis shows that with the increase in load resistance, the frequency splitting phenomenon is suppressed. However, when the frequency splitting phenomenon occurs, the output power can be maintained with a low driving frequency and DC input voltage with Method B. Only the DC input voltage needs to be adjusted when the frequency splitting phenomenon disappears. With Method B, η_{cc} and η_{dd} are not higher than those with Method

A with the same load resistance because maximum efficiency can only be achieved when the driving frequency equals the resonant frequency. Compared with Method A, Method B can fully utilize the system power transfer capacity and can decrease the driving frequency/DC input voltage, which is beneficial in reducing the stress on the switching devices, thereby providing a safe operating condition for the DC–AC inverter.

C. Method C: Adjusting the Coupling Coefficient

When the DC input voltage and driving frequency are held at 100 V and 85 kHz, respectively, changing the coupling coefficient can change the output power of the WPT system to maintain constant output power, as analyzed in the previous section. With the development of mechanization, the coil-to-coil relative position can be accurately adjusted to meet the mutual inductance and coupling coefficient requirements, as shown in Eqs. (39) and (40), which are related to the load resistance.

$$M_{12} = (j\omega_d U_1 + \sqrt{(j\omega_d U_1)^2 - 4(P_{sec}/R_L)\omega_d{}^2 Z_1 Z_2}) /(2\sqrt{P_{sec}/R_L}\omega_d{}^2) \quad (39)$$

$$k = M_{12}/\sqrt{L_1 L_2} \quad (40)$$

Fig. 13 shows the experimental results obtained using Eqs. (39) and (40) to calculate the required coupling factor. FEA software (Maxwell) is used to determine the change in coil separation required to maintain a constant output power (in this case, 1 kW). Tables V and VI show the results in detail. The maximum error of 6.75% occurs in the 25 Ω load condition, and the average error is 4.01%. When the load resistance is changed, adjusting the coil-to-coil distance can achieve constant output power without changing the other parameters.

As discussed in the previous section, when the load resistance or coupling coefficient increases, the load power initially increases and subsequently decreases. However, in this study, the power increase rate caused by the load resistance is much slower than the power increase rate caused by the coupling coefficient. Therefore, with the increase in the load resistance, the coupling coefficient needs to be increased by reducing the coil-to-coil distance. As shown in Fig. 13, when the load resistance increases from 5 Ω to 25 Ω, the coil-to-coil distance decreases from 250 mm to 140 mm to achieve constant output power. With the reduced coil-to-coil distance, η_{cc} and η_{dd} increase from 86.22% to 91.26% and from 77.64% to 86.87%, respectively. The advantage of this method is that the input parameters of the inverter do not need to change, allowing a stable operating condition for the DC–AC inverter. Moreover, with this method, system efficiency increases with the increase in load resistance but may be limited by the coil-to-coil adjustment range.

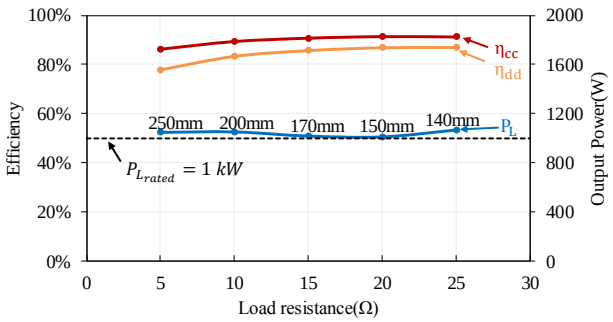

Fig. 13. Experimental results for constant output power by adjusting the coil separation and the coupling coefficient.

TABLE V
CALCULATED COUPLING COEFFICIENT AND CORRESPONDING COIL-TO-COIL DISTANCE DERIVED FROM MAXWELL

R_{La} (Ω)	5	10	15	20	25
$k_{\_req}$	0.1366	0.1926	0.2357	0.2720	0.3041
d (mm)	250	200	170	150	140
$k_{\_FEA}$	0.138	0.19	0.235	0.27	0.29

TABLE VI
MEASURED POWER IN THE EXPERIMENTS

R_{La} (Ω)	5	10	15	20	25
P_{DC} (W)	1,350.9	1,264.9	1,190.9	1,167	1,228.8
P_{pri} (W)	1,307.8	1,228	1,158.2	1,135.7	1,194.5
P_{sec} (W)	1,127.6	1,097.5	1,051.2	1,038.1	1,090.1
P_L (W)	1,048.8	1,052.4	1,019.3	1,012.6	1,067.5
P_{L_exp} (W)	1,000	1,000	1,000	1,000	1,000
Error	4.88%	5.24%	1.93%	1.26%	6.75%

D. Comparative Analysis and Comprehensive Control Method

The previously presented analysis indicates that all of the three methods can achieve a constant output power system and possess their own advantages, limitations, and system performance. We compare the three methods in terms of efficiency because WPT system efficiency is one of the primary objectives of this study. When the efficiencies are compared in a single plot, as shown in Fig. 14, Method A can maintain a nearly stable system efficiency when outputting constant power in the VLWPT system. When the load resistance is small, the system efficiency of Method A is higher than that of the two other methods. However, the lower the load resistance is, the higher the required input DC voltage is, which will lead to high voltage stress on the compensation capacitors, resulting in the need for large capacitor tanks to comply with the high-frequency AC voltage rating. Meanwhile, Method B can effectively utilize the power transfer capacity of the WPT system. By reducing the driving frequency to achieve maximum output power, Method B can also reduce the required DC input voltage, which is beneficial in reducing the stresses on the semiconductor

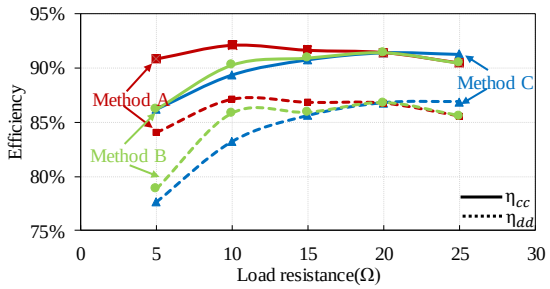

Fig. 14. System efficiency comparison.

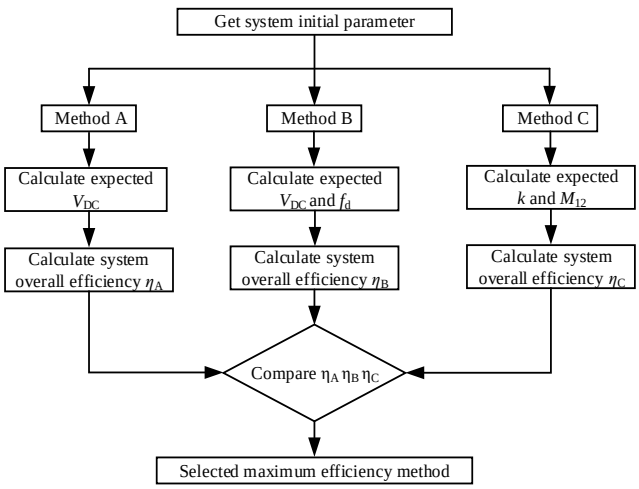

Fig. 15. Effective method selection flowchart.

devices and capacitors. However, with Method B, the WPT system cannot work at the maximum efficiency point (e.g., resonant frequency point), which limits the system efficiency. Moreover, the efficiency of Method B is lower than that of Method A. In Method C, the coil-to-coil distance is usually set as small as possible to provide maximum efficiency. However, a small coil-to-coil distance, that is, an over-coupled condition, seriously limits the output power when the other system parameters are fixed. When system efficiency and output power are considered in the system design, adjusting the coil-to-coil distance for maximum system efficiency may not deliver the desired load power and may require a change in load resistance to achieve the power requirement with an acceptable efficiency. When system efficiency and output power are simultaneously considered in the system design, system efficiency may not reach the maximum to deliver the desired power to the load by tuning the coil-to-coil distance. If the load resistance changes, high system efficiency can be achieved to hold the output power, as shown in this work. Another advantage of Method C is that the inverter operating condition does not change, thus providing the inverter with a highly stable working condition. However, the coil mounting space limits this method.

In conclusion, Methods A and B do not require a change in the coil system and are suitable for VLWTP systems with small load resistance. Method A must sustain a high voltage stress with low load resistance. Method B can fully utilize the system power transfer capacity, but the system efficiency is not higher than that of Method A. Method C is suitable for VLWPT systems with high load resistance and a less space-constrained system. It does not require a change in the operating conditions of the inverter. Therefore, with the proposed comprehensive control method, the coil-to-coil efficiency and overall efficiency can be maintained at approximately 90% and 85%, respectively, in the VLWPT system at 1 kW of output power.

When all of the preconditions of the three methods are satisfied, a comprehensive control method can be selected from them to achieve optimized system efficiency. The flowchart shown in Fig. 15 is based on the mathematical model presented in Section 2.

V. Conclusions

This study provides a mathematical WPT system model with detailed mathematical calculation of the performance of the WPT system. Loss calculation of the power converters is included in the efficiency analysis of the entire WPT system. The coil-to-coil efficiency, overall efficiency, and output power in the WPT system are considered, and the mathematical calculation is validated by experimentation. Three constant output power control methods are presented based on the analysis of WPT system performance and the mathematical WPT system model. These control methods can help validate the accuracy of the proposed mathematical WPT system model and provide a comprehensive control method to achieve high efficiency with constant output power in the VLWPT system. The three methods are validated through experiments, and the advantages and disadvantages of each method are discussed. The results show that with the mathematical WPT system model presented in this study, the system can maintain the expected 1 kW constant power with a maximum error of 6.75% and an average error of 4% when the load resistance varies between 5 and 25 Ω. With the comparison control method, coil-to-coil efficiency and overall efficiency can be maintained at approximately 90% and 85%, respectively, in the VLWPT system.

Acknowledgment

This work is supported by the China Scholarship Council and the National Natural Science Foundation of China (Grant No. 51607179).

References

[1] N. Tesla, “Apparatus for transmitting electrical energy,” U.S. Patent 1119732, Dec.1, 1914.

[2] A. K. RamRakhyani, S. Mirabbasi, and M. Chiao, “Design and optimization of resonance-based efficient wireless

power delivery systems for biomedical implants," *IEEE Trans. Biomed. Circuits Syst.*, Vol. 5, No. 1, pp. 48-63, Feb. 2011.

[3] R. F. Xue, K. W. Cheng, and M. Je, "High-efficiency wireless power transfer for biomedical implants by optimal resonant load transformation," *IEEE Trans. Circuits Syst. I Reg. Papers*, Vol. 60, No. 4, pp. 867-874, Apr. 2013.

[4] A. Zaheer, D. Kacprzak, and G. A. Covic, "A bipolar receiver pad in a lumped IPT system for electric vehicle charging applications," *2012 IEEE Energy Convers. Congr. Expo. ECCE 2012*, No. 1, pp. 283-290, 2012.

[5] U. K. Madawala and D. J. Thrimawithana, "A bidirectional inductive power interface for electric vehicles in V2G systems," *IEEE Trans. Ind. Electron.*, Vol. 58, No. 10, pp. 4789-4796, Oct. 2011.

[6] J. Shin, S, Shin, Y. Kim, S. Ahn, S. Lee, G. Jung, S.-J. Jeon, and D.-H. Cho, "Design and implementation of shaped magnetic-resonance-based wireless power transfer system for roadway-powered moving electric vehicles," *IEEE Trans. Ind. Electron.*, Vol. 61, No. 3, pp. 1179-1192, Mar. 2014.

[7] J. Huh, S. W. Lee, W. Y. Lee, G. H. Cho, and C. T. Rim, "Narrow-width inductive power transfer system for online electrical vehicles," *IEEE Trans. Power Electron.*, Vol. 26, No. 12, pp. 3666-3679, Dec. 2011.

[8] H. Hoang, S. Lee, Y. Kim, Y. Choi, and F. Bien, "An adaptive technique to improve wireless power transfer for consumer electronics," *IEEE Trans. Consum. Electron.*, Vol. 58, No. 2, pp. 327-332, May 2012.

[9] J. C. Lin, "Wireless power transfer for mobile applications, and health effects," *IEEE Trans. Antennas Propag.*, Vol. 55, No. 2, pp. 250-253, Apr. 2013.

[10] Y. D. Lee and S. Y. Park, "Rapid charging strategy in the constant voltage mode for a high power Li-Ion battery," *2013 IEEE Energy Convers. Congr. Expo. ECCE 2013*, pp. 4725-4731, 2013.

[11] T. N. Gucin, M. Biberoglu, and B. Fincan, "A constant-current constant-voltage charging based control and design approach for the parallel resonant converter," *2015 Int. Conf. Renew. Energy Res. Appl. ICRERA 2015*, Vol. 5, pp. 414-419, 2016.

[12] V. B. Vu, V. T. Doan, V. L. Pham, and W. Choi, "A new method to implement the constant current-constant voltage charge of the inductive power transfer system for electric vehicle applications," *2016 IEEE Transp. Electrif. Conf. Expo, Asia-Pacific, ITEC Asia-Pacific 2016*, pp. 449-453, 2016.

[13] N. K. Poon, B. M. H. Pong, and C. K. Tse, "A constant-power battery charger with inherent soft switching and power factor correction," *IEEE Trans. Power Electron.*, Vol. 18, No. 6, pp. 1262-1269, Nov. 2003.

[14] G. a. J. Elliott, G. a. Covic, D. Kacprzak, and J. T. Boys, "A new concept: asymmetrical pick-ups for inductively coupled power transfer monorail systems," *IEEE Trans. Mag.*, Vol. 42, No. 10, pp. 3389-3391, Oct. 2006.

[15] K. W. Klontz, D. M. Divan, D. W. Novotny, and R. D. Lorenz, "Contactless power delivery systems for mining applications." *IEEE Trans. Ind. Appl.*, Vol. 31, No. 1, pp. 27-35, Jan./Feb. 1995.

[16] C. Auvigne, P. Germano, D. Ladas, and Y. Perriard, "A dual-topology ICPT applied to an electric vehicle battery charger," *2012 XXth Int. Conf. Electr. Mach.*, pp. 2287-2292, 2012.

[17] C.-S. Wang, O. H. Stielau, and G. A. Covic, "Design considerations for a contactless electric vehicle battery charger," *IEEE Trans. Ind. Electron.*, Vol. 52, No. 5, pp. 1308-1314, Oct. 2005.

[18] J. G. Hayes, M. G. Egan, J. M. D. Murphy, S. E. Schulz, and J. T. Hall, "Wide-load-range resonant converter supplying the SAE J-1773 electric vehicle inductive charging interface," *IEEE Trans. Ind. Appl.*, Vol. 35, No. 4, pp. 884-895, Jul/Aug. 1999.

[19] G. A. Covic, G. Elliott, O. H. Stielau, R. M. Green, and J. T. Boys, "The design of a contact-less energy transfer system for a people mover system," *PowerCon 2000 - 2000 Int. Conf. Power Syst. Technol. Proc.*, Vol. 1, pp. 79-84, 2000.

[20] R. Mecke and C. Rathge, "High frequency resonant inverter for contactless energy transmission over large air gap," *PESC Rec. - IEEE Annu. Power Electron. Spec. Conf.*, Vol. 3, pp. 1737-1743, 2004.

[21] X. Liu and S. Y. R. Hui, "Optimal design of a hybrid winding structure for planar contactless battery charging platform," *IEEE Trans. Power Electron.*, Vol. 23, No. 1, pp. 455-463, Jan. 2008.

[22] R. Bosshard, J. Muhlethaler, J. W. Kolar, and I. Stevanovic, "The rj-a--Pareto front of inductive power transfer coils," *IECON Proc. (Industrial Electron. Conf.*, pp. 4270-4277, 2012.

[23] S. Li, W. Li, J. Deng, T. D. Nguyen, and C. C. Mi, "A double-sided LCC compensation network and its tuning method for wireless power transfer," *IEEE Trans. Veh. Technol.*, Vol. 64, No. 6, pp. 2261-2273, Jun. 2015.

[24] F. Liu, Y. Yang, D. Jiang, X. Ruan, and X. Chen, "Modeling and optimization of magnetically coupled resonant wireless power transfer system with varying spatial scales," *IEEE Trans. Power Electron.*, Vol. 32, No. 4, pp. 3240-3250, Apr. 2017.

[25] O. Knecht, R. Bosshard, and J. Kolar, "High efficiency transcutaneous energy transfer for implantable mechanical heart support systems," *IEEE Trans. Power Electron.*, Vol. 30, No. 11, pp. 6221-6236, Nov. 2015.

[26] S. Hui, W. Zhong, and F. C. Lee, "A critical review of recent progress in mid-range wireless power transfer," *IEEE Trans. Power Electron.*, Vol. 29, No. 9, pp. 4500-4511, Sep. 2013.

[27] N. Inagaki, "Theory of image impedance matching for inductively coupled power transfer systems," *IEEE Trans. Microw. Theory Tech.*, Vol. 62, No. 4, pp. 901-908, Apr. 2014.

[28] J. M. Miller, P. T. Jones, J. M. Li, and O. C. Onar, "ORNL experience and challenges facing dynamic wireless power charging of EV's," *IEEE Circuits Syst. Mag.*, Vol. 15, No. 2, pp. 40-53, Secondquarter 2015.

[29] J. M. Miller, C. P. White, O. C. Onar, and P. M. Ryan, "Grid side regulation of wireless power charging of plug-in electric vehicles," *2012 IEEE Energy Convers. Congr. Expo. ECCE 2012*, pp. 261-268, 2012.

[30] Y. Wang, Y. Yao, X. Liu, D. G. Xu, and L. Cai, "An LC/S compensation topology and coil design technique for wireless power transfer," *IEEE Trans. Power Electron.*, Vol. 33, No. 3, Mar. 2018.

[31] M. Pinuela, D. C. Yates, S. Lucyszyn, and P. D. Mitcheson, "Maximizing DC-to-load efficiency for inductive power transfer," *IEEE Trans. Power Electron.*, Vol. 28, No. 5, pp. 2437-2447, May. 2013.

[32] Y. Wang, Y. Yao, X. Liu, and D. Xu, "S/CLC compensation topology analysis and circular coil design for

wireless power transfer," *IEEE Trans. Transport. Electrific.*, Vol. 3, No. 2, pp. 496-507, June 2017.
[33] D. Dinu and H. Gietler, "Area efficient charge pump design with constant output power over the whole supply range," *Proc. Int. Semicond. Conf. CAS*, Vol. 2, No. 6, pp. 441-444, 2007.
[34] S. C. Smithson and S. S. Williamson, "Constant power loads in More Electric Vehicles - An overview," *IECON Proc. (Industrial Electron. Conf.*, pp. 2914-2922, 2012.
[35] O. C. Onar, J. M. Miller, S. L. Campbell, C. Coomer, C. P. White, and L. E. Seiber, "A novel wireless power transfer for in-motion EV/PHEV charging," *Conf. Proc. - IEEE Appl. Power Electron. Conf. Expo. - APEC*, pp. 3073-3080, 2013.
[36] H. Wenshan, Y. Lingsong, L. Zhiwei, and Y. Hui, "Loss analysis and improvement of all parts of magnetic resonant wireless power transfer system," *Proc. - 2015 Chinese Autom. Congr. CAC 2015*, pp. 2251-2256, 2016.
[37] S. Dieckerhoff, S. Bernet, and D. Krug, "Power loss-oriented evaluation of high voltage IGBTs and multilevel converters in transformerless traction applications," *IEEE Trans. Power Electron.*, Vol. 20, No. 6, pp. 1328-1336, Nov. 2005.
[38] J. Sallan, J. L. Villa, a. Llombart, and J. F. Sanz, "Optimal design of ICPT systems applied to electric vehicle battery charge," *IEEE Trans. Ind. Electron.*, Vol. 56, No. 6, pp. 2140-2149, Jun. 2009.
[39] S. Moon, B.-C. Kim, S.-Y. Cho, C.-H. Ahn, and G.-W. Moon, "Analysis and design of a wireless power transfer system with an intermediate coil for high efficiency," *IEEE Trans. Ind. Electron.*, Vol. 61, No. 11, pp. 5861-5870, Nov. 2014.
[40] W. Zhong, C. Zhang, X. Liu, and S. Y. R. Hui, "A methodology for making a 3-coil wireless power transfer system more energy efficient than a 2-coil counterpart for extended transmission distance," *IEEE Trans. Power Electron.*, Vol. 30, No. 2, pp. 933-942, Feb. 2015.
[41] A. Pevere, R. Petrella, C. C. Mi, and S. Zhou, "Design of a high efficiency 22 kW wireless power transfer system for EVs fast contactless charging stations," *2014 IEEE Int. Electr. Veh. Conf. IEVC 2014*, 2015.
[42] S. Moon and G.-W. Moon, "Wireless power transfer system with an asymmetric four coil resonator for electric vehicle battery chargers," *IEEE Trans. Power Electron.*, Vol. 31, No. 10, pp. 6844-6854, Oct. 2016.
[43] J. Yin, D. Lin, T. Parisini, and S. Y. Ron Hui, "Front-end monitoring of the mutual inductance and load resistance in a series-series compensated wireless power transfer system," *IEEE Trans. Power Electron.*, Vol. 31, No. 10, pp. 7339-7352, Oct. 2016.
[44] W. Zhong, C. K. Lee, and S. Y. Ron Hui, "General analysis on the use of tesla's resonators in domino forms for wireless power transfer," *IEEE Trans. Ind. Electron.*, Vol. 60, No. 1, pp. 261-270, Jan. 2013.
[45] W. Q. Niu, J. X. Chu, W. Gu and A. D. Shen, "Exact analysis of frequency splitting phenomena of contactless power transfer systems," *IEEE Trans. Circuits Syst.*, Vol. 60, No. 6, pp. 1670-1677, Jun. 2013.
[46] Y. L. Lv, F. Y. Meng, B. J. Che, Y. H. Wu, Q. Wu, and L. Sun, "A novel method for frequency splitting suppression in wireless power transfer," *Proc. 3rd Asia-Pacific Conf. Antennas Propagation, APCAP 2014*, pp. 590-592, 2014.
[47] A. L. Albert, *Radio Fundamentals*, McGraw Hill Book Company Inc, Chap. 4, pp. 101-108, 1948.
[48] F. E. Terman, *Electronic and Radio Engineerin*, McGraw Hill Book Company Inc, Chap. 3, pp. 63-70, 1955.

Xu Liu was born in Jiangsu Province, China, in 1990. He received his B.S. degree from China University of Mining and Technology, Xuzhou, China, in 2012, where he is presently working toward his Ph.D. degree in electrical engineering in the School of Electrical and Power Engineering. He also studies in the University of Bristol as a joint Ph.D. student from 2015 to 2017. His current research interests include wireless power transfer technology and advanced power semiconductors.

Lindsay Clare obtained his B.Sc. degree in electrical and electronic engineering from University College Swansea in 1987 while on special leave from British Telecom. He left British Telecom in 1988 to join GEC-Marconi Avionics, working on switched-mode power supply design. From 1994 to 1998, he worked as a research associate in the Electrical Engineering Department of University of Bristol on an electrical power conditioning project sponsored by DRA, which is now Quinetiq. He returned to the electronics industry in 2003 and rejoined Bristol University as an aerospace electronics technician. He gave up this post in 2005 to take up his present research post. Since then, he has continued to work as a research assistant on various energy-harvesting-related projects and obtained his Ph.D. degree in power conditioning for energy harvesting in 2010. In 2011, he worked on a KTS scheme with SEA on power electronics design. From 2012 to 2013, he served as an RA on the Rotor Testing and Verification Project with Agusta Westland. He rejoined the Electrical Engineering Department at the start of 2014 to work on energy harvesting and power conditioning for the SPHERE project.

Xibo Yuan received his B.S. degree from China University of Mining and Technology, Xuzhou, China, and his Ph.D. degree from Tsinghua University, Beijing, China, in 2005 and 2010, respectively, both in electrical engineering. He is a professor in the Electrical Energy Management Group, University of Bristol, Bristol, UK. His research interests include power electronics and motor drives, wind power generation, multilevel converters, application of wide-bandgap devices, electric vehicles, and other electric aircraft technologies.

Jun Wang received his B.S. degree from Sichuan University, Chengdu, China, and his M.Sc. degree from University of Nottingham, UK, in 2014, both in electrical engineering. He is currently pursuing his Ph.D. degree at Electrical Energy Management Group, University of Bristol, UK. His research interests include power converter topologies, design optimization, and wide-bandgap device applications.

Chonglin Wang was born in Anhui Province, China, in 1956. He received his B.S. degree in electrical engineering and automation and his M.S. and Ph.D. degrees in electrical engineering from CUMT, Xuzhou, China, in 1981, 1989, and 1997, respectively. He has been a professor at the School of Information and Electrical Engineering, CUMT, since 1999. He has also been the chief professor of the Electrical Safety and Intelligent Electrical Equipment Research Institute, CUMT, since 1999. His main research interests are arc suppression coils and electrical safety.

Jianhua Liu was born in Henan Province, China, in 1973. He received his B.S. degree in electrical engineering and automation and his Ph.D. degree in electrical engineering from CUMT, Xuzhou, China, in 1997 and 2008, respectively. He has been with the School of Information and Electrical Engineering, CUMT, since 1999. He is currently an associate professor and a master tutor. His research interests include smart grids, electrical safety, and wireless power transfer systems.